A computational algorithm to simulate disorganization of collagen network in injured articular cartilage

Petri Tanska[1], Petro Julkunen[1,2] and Rami K Korhonen[1,2]

[1]*Department of Applied Physics, University of Eastern Finland, Kuopio, Finland*

[2]*Diagnostic Imaging Center, Kuopio University Hospital, Kuopio, Finland*

Corresponding author:
Petri Tanska, Ph.D.
Department of Applied Physics
University of Eastern Finland
POB 1627, FI-70211 Kuopio
Finland
Tel. +358 50 364 2842
Fax. +358 17 162131
E-mail: petri.tanska@uef.fi

Running title: Modelling collagen disorganization in cartilage

Keywords: Articular cartilage, Finite element analysis, Collagen, Disorganization, Injury, Cartilage mechanics

Abstract

Cartilage defects are a known risk factor for osteoarthritis. Estimation of structural changes in these defects could help us to identify high risk defects, and thus, to identify patients that are susceptible for the onset and progression of osteoarthritis. Here, we present an algorithm combined with computational modeling to simulate the disorganization of collagen fibril network in injured cartilage. Several potential triggers for collagen disorganization were tested in the algorithm following the assumption that disorganization is dependent on the mechanical stimulus of the tissue. We found that tensile tissue stimulus alone was unable to preserve collagen architecture in intact cartilage as collagen network reoriented throughout the cartilage thickness. However, when collagen reorientation was based on both tensile tissue stimulus and tensile collagen fibril strains or stresses, the collagen network architecture was preserved in intact cartilage. Using the same approach, substantial collagen reorientation was predicted locally near the cartilage defect and particularly at the cartilage-bone interface. The developed algorithm was able to predict similar structural findings reported in literature that are associated with experimentally observed remodeling in articular cartilage. The proposed algorithm, if further validated, could help to predict structural changes in articular cartilage following post-traumatic injury potentially advancing to impaired cartilage function.

1. Introduction

In healthy articular cartilage tissue homeostasis is maintained by the equilibrium between degenerative and regenerative processes and strongly contributed by normal mechanical loading. This balance can be disturbed by altered mechanical stimulus of the tissue, for instance due to injurious loading, which may lead to disorganization/fibrillation of the superficial collagen fibril network, proteoglycan loss and osteoarthritis (OA) (Buckwalter and Mankin 1998; Saarakkala et al. 2010). Cartilage proteoglycans (PGs) possess a substantially higher turnover rate (half-life ~3.5 years (Maroudas et al. 1998)) than collagen (half-life ~120 years (Lohmander 1988; Heinemeier et al. 2016)). Therefore, abnormal mechanical stimulus may particularly lead to irreversible changes in the collagen network (Stoop et al. 1999; Karsdal et al. 2008).

Injurious loading of cartilage can induce physical lesions in cartilage (Rolauffs et al. 2010; Alexander et al. 2012; Virén et al. 2012; Myller et al. 2016; Ferizi et al. 2016). It has been suggested that the damage and disorganization of the collagen network could progress following an injury which may further accelerate cartilage degradation (Ferizi et al. 2016). However, it is not known which mechanical signals of cartilage tissue change around a focal cartilage defect that could affect collagen disorganization and possible progression of OA.

Earlier computational studies have demonstrated successfully the formation of an arcade-like Benninghoff-type collagen architecture in intact cartilage in response to normal mechanical loading and swelling pressure (Wilson et al. 2006), and influences of the cartilage composition on the established collagen architecture (Nagel et al. 2013), originating from tissue deformation.

Several investigators have focused on strain/stretch (Driessen 2003; Driessen et al. 2004, 2005, 2008) or stress (Rachev et al. 2000; Taber and Humphrey 2001; Hariton et al. 2007; Driessen et al. 2008) based collagen remodeling in cardiovascular tissues or in other soft tissues in general (Lanir 2015). Furthermore, a recent study suggests that collagen fibril homeostasis might be strain-driven (Oomen et al. 2016), at least in cardiovascular tissues.

In this study, we hypothesized that the disorganization of collagen fibril network could be caused by the changes in the mechanical environment of cartilage resulting from a physical cartilage injury. The hypothesis included the following principal assumptions: 1) collagen architecture must not change in intact cartilage under normal loading (as we assume it homeostatic) and 2) reorientation must be dependent on the mechanical tensile stimulus of the collagen fibrils. In order to investigate our hypothesis, we developed an algorithm capable of evaluating altered collagen fibril orientation resulting from stress and strain stimuli of cartilage matrix and collagen fibrils. The progression of collagen disorganization was then simulated in the models representing intact and mechanically injured (focal defect) cartilage explants.

2. Materials and methods

2.1 Material model

Articular cartilage was modeled based on a fibril-reinforced poroviscoelastic material with Donnan osmotic swelling (FRPVES material) (Wilson et al. 2005b). Briefly, the material model assumes cartilage as a biphasic material consisting of a fluid matrix and a porous solid matrix, which consists of a viscoelastic fibrillar (collagen network) and a swelling non-fibrillar (PG network)

matrices. The collagen fibril network incorporated 4 primary and 13 secondary fibrils. Primary fibrils define Benninghoff-type collagen fibril architecture (Benninghoff 1925) while the secondary fibrils describe randomly organized fibrils and collagen cross-links. The intrinsic tension compression nonlinearity behavior of cartilage (Soltz and Ateshian 2000) was taken into account in the FRPVES material by allowing fibrils only to resist tension. Buckling of the fibrils was assumed to have negligible contribution to mechanical response and was not implemented. The stress of a viscoelastic fibril (σ_f) is given as

$$\sigma_\mathrm{f} = \begin{cases} -\dfrac{\eta}{2\sqrt{(\sigma_\mathrm{f} - E_0\varepsilon_\mathrm{f})E_\varepsilon}}\dot{\sigma}_\mathrm{f} + E_0\varepsilon_\mathrm{f} + \left(\eta + \dfrac{\eta E_0}{2\sqrt{(\sigma_\mathrm{f} - E_0\varepsilon_\mathrm{f})E_\varepsilon}}\right)\dot{\varepsilon}_\mathrm{f}, & \varepsilon_\mathrm{f} > 0, \\ 0, & \varepsilon_\mathrm{f} \le 0, \end{cases} \tag{1}$$

where E_0 and E_ε are the initial and strain-dependent fibril moduli, η is the viscoelastic damping coefficient (viscosity), ε_f is the (logarithmic) fibril strain ($\varepsilon_\mathrm{f} = \ln\left\|\mathbf{F}\cdot\vec{\boldsymbol{e}}_{\mathrm{f},0}\right\|$, see eqs. (2) and (3) for definitions), and $\dot{\sigma}_\mathrm{f}$ and $\dot{\varepsilon}_\mathrm{f}$ are fibril stress and strain rates (*i.e.* $\dot{\sigma}_\mathrm{f} = \frac{\mathrm{d}\sigma_\mathrm{f}}{\mathrm{d}t}$ and $\dot{\varepsilon}_\mathrm{f} = \frac{\mathrm{d}\varepsilon_\mathrm{f}}{\mathrm{d}t}$).

The stress tensor for an individual fibril is of a form

$$\boldsymbol{\sigma}_\mathrm{f}^{i} = \begin{cases} \rho_\mathrm{z} C\sigma_\mathrm{f}\vec{\boldsymbol{e}}_\mathrm{f}\otimes\vec{\boldsymbol{e}}_\mathrm{f}, & \text{for primary fibrils,} \\ \rho_\mathrm{z}\sigma_\mathrm{f}\vec{\boldsymbol{e}}_\mathbf{f}\otimes\vec{\boldsymbol{e}}_\mathrm{f}, & \text{for secondary fibrils,} \end{cases} \tag{2}$$

where ρ_z is the depth-dependent total collagen fraction per solid volume, C (=12.16) is the ratio between primary and secondary fibrils and it has been obtained earlier for this fibril-reinforced material (see more details from (Wilson et al. 2004, 2005b, a)), ⊗ denotes a dyadic product and

$\vec{\boldsymbol{e}}_{\mathrm{f}}$ is the current fibril orientation calculated from the initial fibril orientation ($\vec{\boldsymbol{e}}_{\mathrm{f},0}$; a unit vector) as follows

$$\vec{\boldsymbol{e}}_{\mathrm{f}} = \frac{\mathbf{F} \cdot \vec{\boldsymbol{e}}_{\mathrm{f},0}}{\left\| \mathbf{F} \cdot \vec{\boldsymbol{e}}_{\mathrm{f},0} \right\|}, \tag{3}$$

where **F** is the deformation gradient tensor.

The stress tensor of the non-fibrillar matrix was defined based on the strain density function of a Neo-Hookean material

$$\boldsymbol{\sigma}_{\mathrm{m}} = K_{\mathrm{m}} \frac{\ln(J)}{J} \mathbf{I} + \frac{G_{\mathrm{m}}}{J} \left(\mathbf{F} \cdot \mathbf{F}^{T} - J^{2/3} \mathbf{I} \right), \tag{4}$$

where K_{m} and G_{m} are bulk and shear moduli, J is the determinant of the deformation gradient tensor and **I** is unit tensor. Fluid flow inside the porous solid matrix was modeled based on Darcy's law and permeability was implemented as deformation-dependent based on changes in void ratio according to van der Voet (van der Voet 1997),

$$k = k_0 \left(\frac{1 + e}{1 + e_0} \right)^{M}, \tag{5}$$

where k and k_0 are the current and initial hydraulic permeabilities, e and e_0 are the current and initial void ratios and M is a positive constant describing the strain-dependency of the permeability.

The tissue swelling was based on the Donnan osmotic swelling pressure gradient which can be determined at equilibrium as follows

$$\Delta\pi = \phi_{\mathrm{int}} RT \left(\sqrt{c_{\mathrm{F}}^2 + 4 \frac{\left(\gamma_{\mathrm{ext}}^{\pm}\right)^2}{\left(\gamma_{\mathrm{int}}^{\pm}\right)^2} {c_{\mathrm{ext}}}^2} \right) - 2\phi_{\mathrm{ext}} RT c_{\mathrm{ext}}, \tag{6}$$

where ϕ_{ext}, ϕ_{int}, $\gamma_{\mathrm{ext}}^{\pm}$, $\gamma_{\mathrm{int}}^{\pm}$ are external and internal osmotic coefficients and external and internal activity coefficients, respectively, c_{ext} is external salt concentration (0.15 M), R is the molar gas constant and T is the absolute temperature (293 K).

The total stress tensor of the FRPVES material can now be stated as a sum of the individual stress tensors of the constituents as

$$\boldsymbol{\sigma}_{\mathrm{t}} = \sum_{i=1}^{totf} \boldsymbol{\sigma}_{\mathrm{f}}^{i} + \boldsymbol{\sigma}_{\mathrm{m}} - (\Delta\pi + \mu_{\mathrm{f}})\mathbf{I}, \tag{7}$$

where *totf* is the total number of fibrils and μ_{f} is the chemical potential of water. The term $\Delta\pi + \mu_{\mathrm{f}}$ is equal to fluid pressure p in poroelastic/biphasic materials. Structural, compositional and material parameters are presented in Table 1. For more detailed description of the material model, please see Wilson *et al.* (Wilson et al. 2005b) and Tanska *et al.* (Tanska et al. 2013), and for the implementation of the collagen fibril network architecture, please see Supplementary material.

Table 1. Material, compositional and structural parameters for the fibril reinforced poroviscoelastic swelling (FRPVES) cartilage.

Material parameter	**Value**	**Description**
E_0 (MPa)	2.737*	Initial fibril modulus
E_ε (MPa)	867.7*	Strain-dependent fibril modulus
η (MPa·s)	1418*	Collagen fibril damping coefficient (viscosity)
C (-)	12.16**	Ratio of primary to secondary collagen fibrils
E_m (MPa)	0.315**	Non-fibrillar matrix modulus
ν_m (MPa)	0.01**	Poisson's ratio of the non-fibrillar matrix
k_0 (10^{-15} m^4/(Ns))	1.522**	Initial permeability
M (-)	1.339**	Permeability strain-dependency coefficient
Composition		
n_f (-)	0.8-0.15z***	Depth-dependent fluid fraction
c_f (mEq/ml)	-0.1z^2+0.24z+0.035**	Depth-dependent fixed charge density
ρ_z (-)	1.4z^2-1.1z+0.59**	Depth-dependent collagen fraction
Structure		
d_sup	0.12h†	Superficial zone thickness
d_mid	0.26h†	Middle zone thickness
d_deep	0.62h†	Deep zone thickness

*Obtained from Wilson *et al.*(Wilson et al. 2005b)
**Obtained from Wilson *et al.*(Wilson et al. 2005a)
***Obtained from Mow *et al.*(Mow and Guo 2002).
†Obtained from Julkunen *et al.*(Julkunen et al. 2007)
z indicates normalized distance from the cartilage surface (surface = 0, cartilage-bone interface = 1)
h indicates cartilage thickness

2.2 Collagen reorientation algorithm

Earlier computational studies by Driessen *et al.* (Driessen 2003; Driessen et al. 2005, 2008), Menzel (Menzel 2007), Nagel and Kelly (Nagel et al. 2013), Wilson *et al.* (Wilson et al. 2006) and an experimental study by Oomen *et al.* (Oomen et al. 2016) have proposed that collagen fibrils align according to a tensile strain. To test our hypothesis that the reorientation of the collagen fibrils could be caused by the changes in the mechanical environment of cartilage resulting from a physical cartilage injury, we incorporated the approach based on the study by Wilson *et al.* (Wilson

et al. 2006) and further modified it and tested with different mechanical signals. In this study, the fibrils were assumed to orient with respect to the undeformed (reference) state, and thus, the tensile stimulus in the cartilage tissue was evaluated in a Lagrangian frame either from the Green-Lagrangian strain tensor **E** (similarly as in Wilson *et al*. (Wilson et al. 2006)) defined as

$$\mathbf{E} = \frac{1}{2}(\mathbf{C} - \mathbf{I}), \tag{8}$$

where **C** is the right Cauchy-Green deformation tensor (**C** = $\mathbf{F}^{\mathrm{T}}\cdot\mathbf{F}$), or from the 2nd Piola-Kirchhoff stress tensor $\mathbf{S}_{2\mathrm{PK}}$ (our additional hypothesis) obtained through a pull-back operation of the Cauchy stress tensor $\boldsymbol{\sigma}_{\mathrm{c}}$ (stress output in Abaqus and equivalent to the total stress in eq. (7)):

$$\mathbf{S}_{2\mathrm{PK}} = J\,\mathbf{F}^{-1}\boldsymbol{\sigma}_{\mathrm{c}}\mathbf{F}^{-\mathrm{T}}. \tag{9}$$

The approach in equation (9) has been previously used for cardiovascular tissues (Rachev et al. 2000; Taber and Humphrey 2001; Hariton et al. 2007), but not in cartilage. Using spectral decomposition, these strain and stress tensors can be decomposed into their principal strain/stress values λ_i (eigenvalues) and corresponding principal strain/stress directions $\vec{\boldsymbol{n}}_i$ (eigenvectors). Now the collagen fibril is reoriented towards a preferred fibril direction $\vec{e}_{\mathrm{p}}$, which is defined as follows (Driessen et al. 2005; Wilson et al. 2006; Hariton et al. 2007)

$$\vec{e}_{\mathrm{p}} = \frac{g_1\vec{\boldsymbol{n}}_1 \pm g_2\vec{\boldsymbol{n}}_2 \pm g_3\vec{\boldsymbol{n}}_3}{\sqrt{{g_1}^2 + {g_2}^2 + {g_3}^2}}, \tag{10}$$

where g_i are the functions of the principal strain or stress (in the Lagrangian frame) as follows

$$\begin{cases} g_i = \lambda_i, & \lambda_i > 0, \\ g_i = 0, & \lambda_i \leq 0, \end{cases} \tag{11}$$

i.e., only positive (tensile) tissue strains/stresses are contributing to the fibril disorganization. Eq. (10) results in four $\vec{e}_{\mathrm{p}}$ vectors which ensures the symmetry of the primary fibril architecture. Now, the fibril is rotated around the rotation axis $\vec{\boldsymbol{k}}$ defined as

$$\vec{\boldsymbol{k}} = \frac{\vec{\boldsymbol{e}}_{\mathrm{f},0} \times \vec{\boldsymbol{e}}_{\mathrm{p}}}{\left\| \vec{\boldsymbol{e}}_{\mathrm{f},0} \times \vec{\boldsymbol{e}}_{\mathrm{p}} \right\|}, \tag{12}$$

where $\vec{e}_{\mathrm{f},0}$ is the fibril direction in the undeformed configuration. By utilizing the matrix exponential, the new fibril direction ($\vec{\boldsymbol{e}}_{\mathrm{f,new}}$; a unit vector) can be calculated as follows:

$$\vec{\boldsymbol{e}}_{\mathrm{f,new}} = \exp(\kappa\alpha\widehat{\mathbf{K}})\vec{\boldsymbol{e}}_{\mathrm{f},0}, \tag{13}$$

where κ is a positive constant for the rate of reorientation (from 0 to 1), $\alpha = \arccos\left\| \vec{\boldsymbol{e}}_{\mathrm{f},0} \cdot \vec{\boldsymbol{e}}_{\mathrm{p}} \right\|$ is the angle $\vec{\boldsymbol{e}}_{\mathrm{f},0}$ and $\vec{\boldsymbol{e}}_{\mathrm{p}}$ (calculated from eq. (10)) and $\widehat{\mathbf{K}}$ is the cross-product matrix of $\vec{\boldsymbol{k}}$. Aforementioned calculations are determined for each primary–preferred fibril direction pair and the fibril is rotated towards the closest preferred direction. Then, the new fibril directions are updated and a new iteration (mechanical and reorientation analysis) is started.

2.3 Finite element simulations

Two 3D FE models representing cylindrical osteochondral explants (h = 1.5 mm, r = 1.5 mm, Figure 1) were constructed (element type C3D8P) using FRPVES material implemented using

UMAT subroutine in ABAQUS 6.13 (Dassault Systèmes, Providence, RI, USA). The *reference model* was kept intact while the *injury model* included a 20 μm wide and 750 μm deep lesion throughout the explant in order to investigate the effect of a focal defect (change in the mechanical environment) on collagen architecture following injurious loading (Virén et al. 2012). In both models, the bottom nodes were fixed (*i.e.* no rotation or translation degrees of freedom were allowed) to simulate rigid subchondral bone. Fluid flow though free cartilage surfaces was allowed (pore pressure = 0) while other surfaces were sealed. The contact between cartilage and rigid and impermeable platen was modeled using *surface-to-surface* formulation with a finite sliding and hard pressure-overclosure relationship. Coefficient of friction was set to 0.1 (Teeple et al. 2008).

Following an initial free-swelling step (to establish mechanical equilibrium and pre-strain in collagen network), a ramp load of 2 MPa for 0.1 s was applied on the cartilage surface in an unconfined compression geometry (Figure 1A & B). The magnitude and duration of the load were selected to correspond to physiologically relevant loading, *i.e.*, they can represent typical values during the loading response of the gait (Brand 2005; Yang et al. 2010; Gilbert et al. 2014; Tanska et al. 2015; Kłodowski et al. 2016). Similar values have also been used in other computational studies (Zhang et al. 2015). In addition, in order to approximate the influence of sliding that occurs in the knee joint, the effect of shear loading on the disorganization process in the *reference* and *injury models* was investigated by applying a sliding of 40 mm/s for 0.1 s following the compression (Figure 1C). At the end of the application of the load, the deformation gradient and Cauchy stress tensors, *i.e.,* deformation and stress of the whole cartilage tissue matrix, were obtained using URDFIL subroutine in ABAQUS. Based on the study by Wilson et al. (Wilson et

al. 2006), 1) time incrementally averaged Cauchy-Green deformation tensor and 2) the maximal right Cauchy-Green deformation tensors produced practically identical results for the remodeling. This was also verified by our preliminary simulations. Thus, the maximal strain or stress tensor at the end of the simulation was selected to drive the reorientation process in a custom-made Matlab script (R2014a, The MathWorks, Inc., Natick, MA, USA). In contrast to our hypothesis, it was also observed in our preliminary simulations that the normal Benninghoff-type architecture was not preserved if only the strain or stress of the solid matrix was taken into account (parameters from elements). Consequently, an additional constraint was included as follows:

$$\begin{cases} \kappa = 0.3, & \varepsilon_{\mathrm{f}} > 0 \\ \kappa = 0, & \varepsilon_{\mathrm{f}} \leq 0, \end{cases} \tag{14}$$

i.e. the reorientation to occur only if the strains in the collagen fibrils were in tensile direction (fibrillar matrix experiences tension). The value κ = 0.3 was selected based on our preliminary simulations and a previous study (Wilson et al. 2006) which enabled the optimal convergence for the fibril reorientation. In other cases, without the additional constraint, the reorientation rate was set to κ = 0.3 and fibril homeostasis (no reorientation) was assumed when $\alpha < 1°$. Finally, the collagen network architecture was evaluated after 50 consecutive iterations, as the principal stress or strain values at the middle zone of cartilage were close to equal which sometimes led to local instabilities. In these points the remodeling was not allowed to occur, thus, the algorithm was allowed to run sufficiently long (50 iterations) to ensure that the instabilities do not affect the outcome of the simulation and an equilibrium condition was reached. The mesh convergence was also verified using eight times denser mesh (difference between stress and strain values < 5 %).

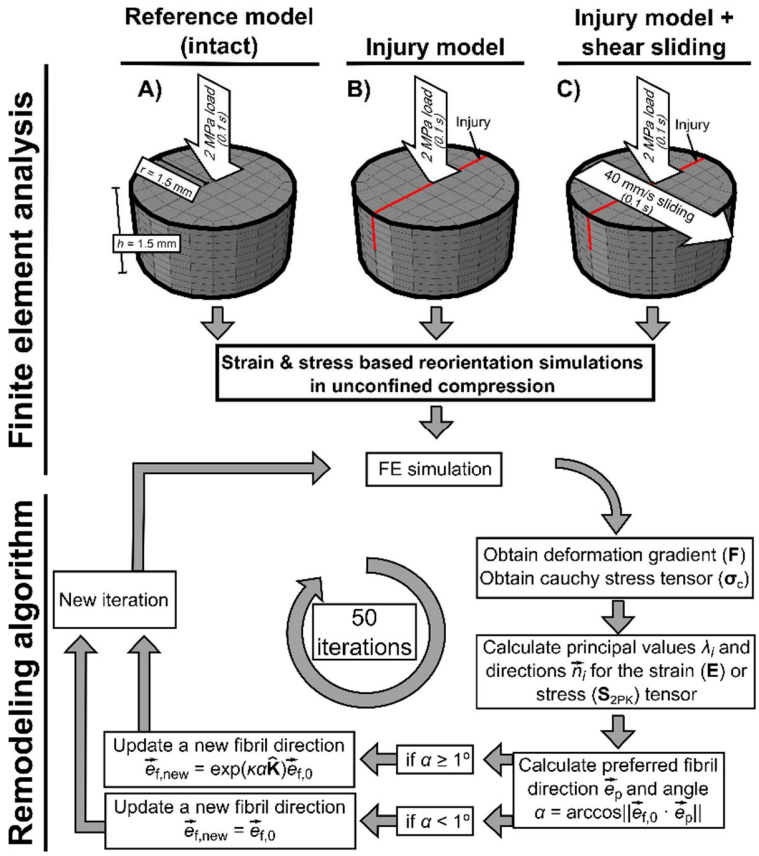

Figure 1: Sample geometries for the finite-element models representing osteochondral explants and the remodeling procedure. Following a free-swelling step, A) reference (intact) and B) injured explants were subjected to a 2 MPa load for 0.1 s. In addition, C) intact and injured explants (only injured shown) were also subjected to a sliding of 40 mm/s for 0.1 s following the 2 MPa loading. After the mechanical simulation, the deformation gradient and Cauchy stress tensors were obtained, converted to the Lagrangian frame and used for driving the collagen reorientation algorithm (bottom figure) and new orientations were implemented to the mechanical analysis. This procedure was repeated 50 times and fibril homeostasis was verified with visual inspection.

3. Results

3.1 Fibril reorientation with tensile tissue strain based algorithm

The superficial collagen architecture was simulated to extend over 50% of the total thickness of the intact *reference model* when compared to initial orientation angles (Figure 2A, i). In the *injury model*, the architecture was simulated to become closer to 45° orientation angle near and along the injury bottom edge compared to the intact *reference model.* In addition, the architecture was simulated to remain nearly unchanged near the bone-cartilage interface (Figure 2A, i). When the *injury model* was subjected to additional shear sliding, the orientation angles were closer to 45° even in larger areas near and along the injury bottom edge when compared to the intact *reference model* and *injury model* (Figure 2A, i). A more detailed examination of the orientation angles at the center of the explant next to the injury location revealed that the orientation angle differences between the models were negligible (Figure 3A, blue lines).

3.2 Fibril reorientation with tensile tissue strain and tensile fibril strain based algorithm

The initial collagen architecture was well-preserved throughout the intact *reference model*; the orientation angles were changed only near the bone cartilage interface where they changed slightly closer to 45° when compared to the initial orientation angles (Figure 2A, ii). Again, the presense of the injury changed orientation angles near and along the injury bottom edge closer to 45° compared to the intact *reference model*, while sliding in the *injury model with shear sliding* further amplified this change in larger area (Figure 2A, ii). Similar finding was also observed in a more detailed examination of the orientation angles at the center of the explant next to the injury (Figure 3A, red lines).

3.3 Fibril reorientation with tensile tissue stress based algorithm

The collagen architecture was simulated to resemble close to the one in the corresponding strain based method in the intact *reference model* (i.e., the orientation angles that are typically present in superficial cartilage occupied over 50% of the cartilage thickness), except for a slight change in the orientation angles at the normalized depths from 0.15 to 0.4, where orientation angles were changed closer to 45° (Figure 2B, ii and Figure 3B blue lines). Instead in the *injury model*, the collagen architecture below the defect changed even closer to 45°, while near the bone-cartilage interface the orientation remained the same compared to the *reference model* (Figure 2A, ii and Figure 3B blue dash line). This was also the case in the *injury model with shear sliding,* except that the orientation near the bottom of the injury edge became slightly more aligned along with the injury bottom edge when compared to the *injury model* (Figure 2B, iii and Figure 3B blue dash-dot line).

3.4 Fibril reorientation with tensile tissue stress and tensile fibril strain based algorithm

The initial architectire was completely preserved in the *reference model* (Figure 2B, iv). In the *injury model* (Figure 2B, iv and Figure 3B, red dashed line) and *injury model with shear sliding* (Figure 2B, iv and Figure 3B, red dash-dot line), the orientation of the collagen network was changed slighly near the bone-cartilage interface, while at the other cartilage depths the architecture remained close to the same with the *reference model* (Figure 2B, iv and Figure 3b, red lines).

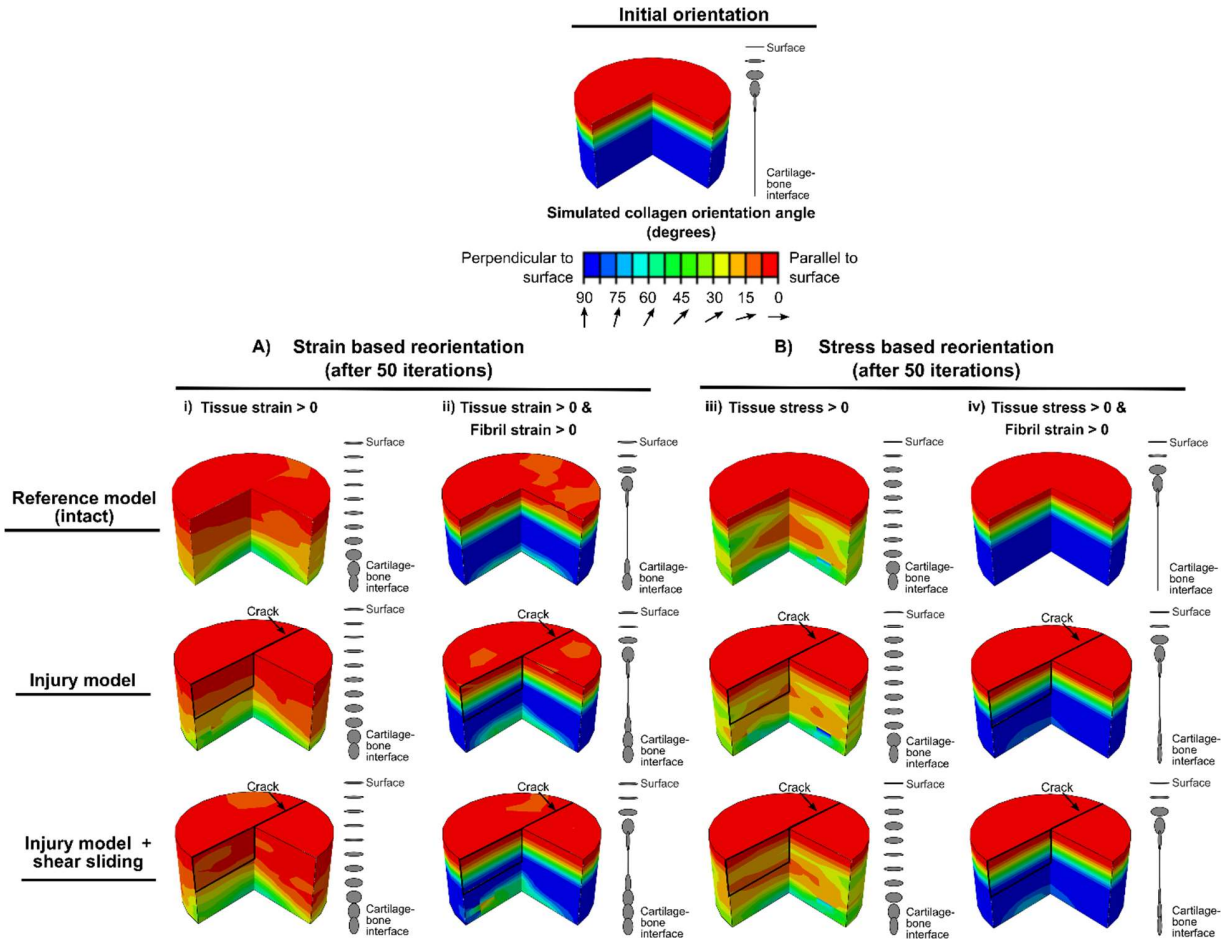

Figure 2: Spatial distribution and corresponding elliptical representation (from the center of the explant) of the orientation angles after 50 iterations using the tensile strain (A, i) or stress (B, iii) of the tissue as a driven parameter for the collagen fibril reorientation algorithm. Based on the preliminary simulations, it was observed that the normal Benninghoff-type architecture was not preserved if only the strain or stress of the tissue was taken into account in the algorithm. Consequently, an additional constraint was included to the algorithm by allowing the reorientation to occur only if the strains in the collagen fibrils were in tensile direction in addition to the tensile strain (A, ii) or stress (B, iv) in the tissue. Injury sites (focal defects) are marked with black lines. Application of the shear loading on the reference model produced negligible differences with respect to the shown reference model, thus, the results are not shown.

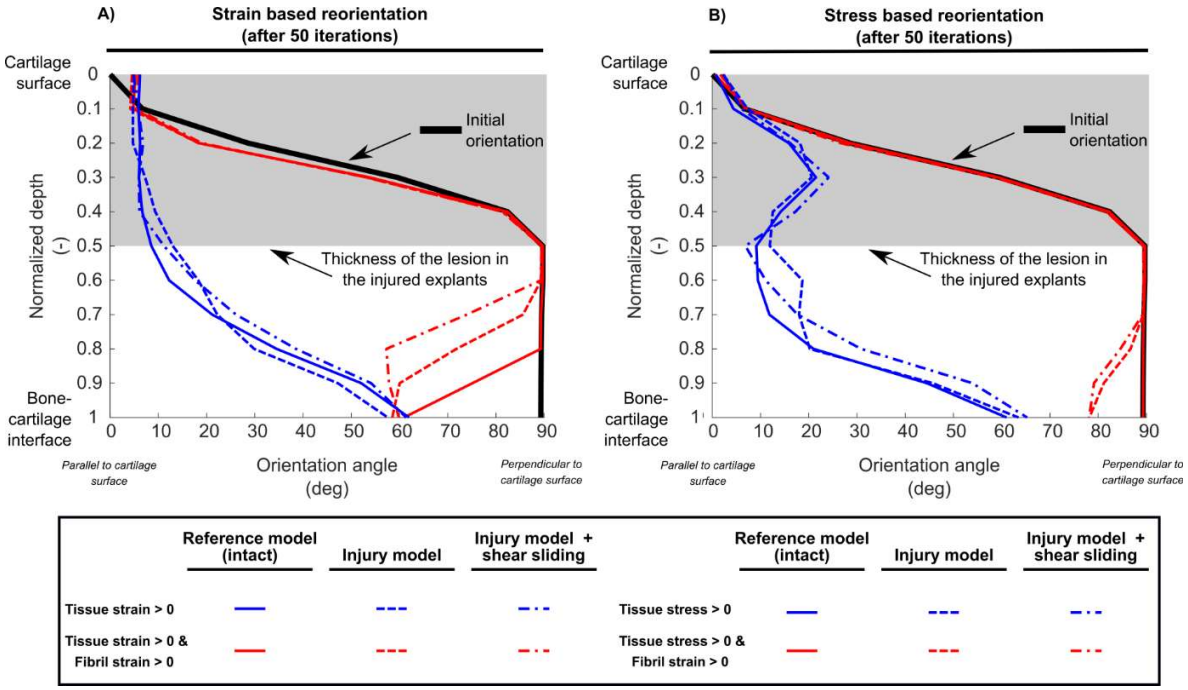

Figure 3: Collagen network orientation profiles from the center of the explant using A) the strain based and B) stress based reorientation algorithms resulting solely from tissue strain/stress stimulus (blue lines) and from tissue strain/stress stimulus with collagen fibrils experiencing tensile stimulus (red lines). Initial orientation is presented as a black line and the depth of the focal lesion as shaded area. Application of the shear loading on the reference model produced negligible differences with respect to the shown reference model, thus, the results are not shown.

4. Discussion

4.1 Summary

The collagen fibril reorientation algorithm, based on a tensile tissue strain or stress stimulus and collagen fibril strain, was used for investigating the potential reorientation/disorganization of the collagen fibril network due to the focal cartilage lesion. Cartilage tissue was modeled as a fibril-reinforced biphasic material capable to separate contributions of the non-fibrillar and fibrillar matrices on cartilage mechanics. The collagen reorientation was then simulated in the models representing intact and injured cartilage (half-thickness lesion). We found that tissue stress or

strain based reorientation approaches predict reorientation of the collagen network. If these reorientation approaches were bounded by an extra condition that the collagen fibrils must experience tensile strain, the Benninghoff type collagen architecture was preserved in most of the tissue, and in the injured tissue, most of the reorientation was observed near the bone-cartilage interface and below the lesion.

4.2 Alterations in cartilage structure simulated by the reorientation algorithm

Using purely the tissue stress or strain as the driving factor for the reorientation process, the superficial collagen architecture occupied more than half of the thickness of the intact and injured cartilage explant. This could be potentially explained by the unconfined compression geometry as the tissue can only expand in the transversal direction. This same could potentially occur also *in vivo* but we did not test that here. The unconfined geometry was chosen as it is relatively easy to apply *in vitro* for large number of samples (see e.g. (Li et al. 2013)). Yet, we acknowledge that the loading in unconfined geometry can be considered as an idealization and *in vivo* loading on cartilage is more complex and may vary from subject to subject.

If the reorientation was allowed to occur only when both tissue and collagen fibrils experienced tensile stimulus (collagen fibrils were assumed to only resist tension, see eq. (1)), both strain and stress based disorganization methods predicted nearly unchanged arcade-like architecture in the intact *reference model*. Interestingly, the degree of collagen disorganization increased near the bone-cartilage interface in the *injury model*. In addition, when the *injury model* was subjected to shear sliding, the level of disorganization was slightly more amplified in the strain based algorithm

and it progressed closer to the bottom of the lesion. These findings suggest that the tensile stimulus of collagen network could be important to consider in future adaptive modeling approaches as they might play a role in cartilage adaptation.

4.3 Comparison to literature

Our findings are partially supported by an experimental *ex vivo* study (Lyman et al. 2012) in which the fibrillation of collagen fibril network was observed to occur near the experimentally produced partial-thickness defects over a 4-week period (localized at the superficial and deep zones). Similar findings have also been reported in an *in vitro* injury study (Rolauffs et al. 2010) and an *in vivo* study of cartilage repair in goats (Raub et al. 2013). In the former study, significant collagen crimping was localized at the deep tissue and no crimping was observed at the superficial tissue 48 hours after the injury. In the latter study, localized remodeling of the collagen network was observed in adjacent host and implanted repair cartilage in goats 6 months after the repair operation. This experimental remodeling in goats was found to be consistent with the direction and magnitude of cartilage strain resulting collagen network remodeling from the orientation angles of ~85° in non-operated controls closer to 45° orientation angle in repaired tissue near the bone-cartilage interface, and below and next to the defect (repair area). Moreover, diffusion tensor MRI based measurements in injured cartilage have shown a decrease of fractional anisotropy (Ferizi et al. 2016) that can be related to the more disorganized collagen architecture, i.e., reorientation closer to the 45° orientation angles in the current model. Yet, it is not certain whether this experimentally observed decrease in the fractional anisotropy results from either disorganization/reorientation of collagen network or loss of proteoglycans or both. There are also some computational (Venäläinen

et al. 2016) and *in vivo* experimental (Myller et al. 2016) studies with clinical data showing that cartilage lesions cause substantial and significant changes, respectively, at the deep tissue below and near cartilage lesion. However, these changes should be verified in more detail with carefully planned *in vitro* and *in situ* experiments as quantification of these changes remains as a challenge when considering the resolution of current clinical imaging modalities, especially in investigations of longitudinal changes due to controlled remodeling.

4.4 Limitations

It is possible that the collagen reorientation process is relatively slow which occurs during several months or even years and that *in vivo* loading is not always the same. These factors might partially explain why most short-term cyclic loading *in vitro* studies have not observed radical changes in collagen orientation (Kääb et al. 1998). Because of these factors, we chose to represent this characteristic time (which is challenging to verify) for the remodeling process as a normalized constant (κ). Thus, the time scale in our algorithm is currently arbitrary (iterations).

The loading protocol (a ramp load of 2 MPa in 0.1 s) was a simplification of a physiologically relevant loading such as that during the loading response of the gait cycle (Brand 2005; Yang et al. 2010; Gilbert et al. 2014; Tanska et al. 2015; Korhonen et al. 2015; Kłodowski et al. 2016). However, based on Wilson et al. (Wilson et al. 2006), deformation based remodeling is not sensitive to the duration and frequency of the applied loading, but is dependent on the magnitude of the load (Nagel et al. 2013) and probably also on the type of the contact properties (e.g. friction,

sliding). Thus, greater loading force and higher friction during sliding would just amplify our results.

The collagen reorientation was assumed to result solely from the changes in the mechanical signals of cartilage and collagen. The reorientation (which could also be considered as disorganization) might also result from breakdown of the collagen fibrils in the close proximity of the injury following injurious loading which was not considered directly in the algorithm. On the other hand, the collagen damage was taken into account in the injured geometry.

The position (Venäläinen et al. 2016) and presumably size and shape of the tissue defect modulate the mechanical environment around the defect in a human knee joint, which can result in different strain and stress directions. This changed local mechanical environment can also lead to stress concentrations at the superficial cartilage and/or near the lesion, which have been suggested to lead to the breakdown and degeneration of the collagen matrix (Sasazaki et al. 2006; Hosseini et al. 2014; Mononen et al. 2016), which could potentially contribute to the collagen fibrillation.

The viscoelastic fibril definition was mainly chosen as it is validated earlier (Wilson et al. 2004, 2005b, a). The viscoelasticity contributes also to the time-dependent mechanical response of cartilage and, thus, also to the time-invariant remodeling process presented in this study. We believe that quite similar results could be achieved with non-linear elastic fibrils and correct selection of the material parameters.

4.5 Future developments

Unconfined compression geometry did not include subchondral bone. However, based on recent clinical and computational studies (Hart et al. 1991; Venäläinen et al. 2014, 2016), bone could be important to consider when simulating the physiological environment of cartilage as changes in subchondral bone density and plate thickness might alter the strain and stress distribution in cartilage, thus, possibly contributing to the changes in the collagen network structure in injured cartilage during the progression of OA. In addition, depth-wise and spatial variation in the material properties and composition of cartilage might affect slightly to the simulation results, especially if they are changed during the reorientation process. In order to take these material level properties into account, direct experimental data following cartilage injury should be collected.

In addition to changes in the collagen network, the cartilage matrix goes through several changes during OA. Especially, cartilage injury can cause inflammation and cytokine release which may lead particularly to diminished PG formation. There can also be direct PG loss due to collagen damage or cell death related PG loss around the lesion. These factors were not taken into account in our algorithm. On the other hand, a recent follow-up study (Neuman et al. 2017) investigating synovial fluid biomarkers in the development of OA found that concentration of inflammation related biomarkers was elevated within 2 weeks after an anterior cruciate ligament injury, while the concentration was normalized during the following year and remained nearly unchanged during the follow-up period of 7 years. These subjects developed radiographical OA during the 16 year follow-up, but the development was not related to the biomarkers (Neuman et al. 2017). It may be possible that the inflammation initially disturbs the normal integrity of the cartilage making it more prone to further progression of OA caused by long term mechanical loading. On the other

hand, inflammation-induced cartilage degradation can be rather related to PGs than collagen. PG loss would change the mechanical properties and stress/strain states of cartilage around the lesion. In the future, anabolic and catabolic activities of cells and following PG degradation and formation should be included into the algorithm. This would necessitate in vitro follow-up data of several mechanisms simultaneously following injurious loading.

Computational simulations have also shown that fluid phase can support around 80% of the cartilage load during and immediately after the load application (Li et al. 2014; Quiroga et al. 2017). If the load experienced by cartilage increases (e.g. due to partial or total meniscectomy (Bedi et al. 2010, 2012)), it may first cause increased contact and fluid pressure and then a relatively rapid consolidation. This can also be seen as a decrease of fluid pressure slightly after the application of the load (Kazemi et al. 2013; Miramini et al. 2017). If cartilage is additionally damaged, its ability to sustain fluid pressurization for a long periods of time may be compromised (Dabiri and Li 2015; Miramini et al. 2017), which may subject the tissue to excessive strains leading to matrix damage and chondrocyte death. These phenomena may further contribute to the collagen remodeling and tissue failure, and should be investigated in more detail.

4.6 Conclusions

In conclusion, the presented collagen reorientation algorithm, based on tissue stress/strain together with collagen fibril tensile strain, was able to predict collagen reorientation near the cartilage defect and close to the bone-cartilage interface. In the future, this algorithm, when validated, may be utilized as a potential tool to predict the progression of OA related changes in the knee joint, and

could in optimal case aid in optimizing loading and rehabilitation protocols to restore normal cartilage function.

Role of the funding source

The research leading to these results has received funding from the European Research Council under the European Union's Seventh Framework Programme (FP/2007–2013), ERC Grant Agreement no. 281180, the Academy of Finland (projects 286526, 305138), State Research Funding from Kuopio University Hospital (project 5041763), Sigrid Juselius Foundation, Finnish Cultural Foundation North Savo regional fund (grant 65142194) and Alfred Kordelin Foundation (grant 150465). The funding sources had no role in the study design, collection, analysis and interpretation of data; in the writing of the manuscript; and in the decision to submit the manuscript for publication.

Acknowledgments

CSC—IT Center for Science Ltd., Finland is acknowledged for providing modeling software and Mikko S. Venäläinen, Ph.D., for technical support.

Contributions

PT: The conception and design of the study, acquisition of data, analysis and interpretation of data. Drafting and critical revision of the article for intellectual content. **PJ:** The conception and

design of the study, analysis and interpretation of data. Drafting and critical revision of the article for intellectual content.

RKK: The conception and design of the study, analysis and interpretation of data. Drafting and critical revision of the article for intellectual content.

Conflict of Interest

The authors declare that they have no conflict of interest.

References

Alexander PG, McCarron JA, Levine MJ, et al (2012) An In Vivo Lapine Model for Impact-Induced Injury and Osteoarthritic Degeneration of Articular Cartilage. Cartilage 3:323–333. doi: 10.1177/1947603512447301

Bedi A, Kelly N, Baad M, et al (2012) Dynamic contact mechanics of radial tears of the lateral meniscus: implications for treatment. Arthroscopy 28:372–81. doi: 10.1016/j.arthro.2011.08.287

Bedi A, Kelly NH, Baad M, et al (2010) Dynamic contact mechanics of the medial meniscus as a function of radial tear, repair, and partial meniscectomy. J Bone Joint Surg Am 92:1398–408. doi: 10.2106/JBJS.I.00539

Benninghoff A (1925) Form und Bau der Gelenkknorpel in ihren Beziehungen zur Funktion. Z Anat Entwicklungsgesch 76:43–63. doi: 10.1007/BF02134417

Brand RA (2005) Joint contact stress: a reasonable surrogate for biological processes? Iowa Orthop J 25:82–94.

Buckwalter JA, Mankin HJ (1998) Articular cartilage: degeneration and osteoarthritis, repair, regeneration, and transplantation. Instr Course Lect 47:487–504. doi: 9571450

Dabiri Y, Li LP (2015) Focal cartilage defect compromises fluid-pressure dependent load support in the knee joint. Int j numer method biomed eng 31:659–80. doi: 10.1002/cnm.2713

Driessen NJB (2003) Computational Analyses of Mechanically Induced Collagen Fiber Remodeling in the Aortic Heart Valve. J Biomech Eng 125:549. doi: 10.1115/1.1590361

Driessen NJB, Bouten CVC, Baaijens FPT (2005) Improved Prediction of the Collagen Fiber Architecture in the

Aortic Heart Valve. J Biomech Eng 127:329. doi: 10.1115/1.1865187

Driessen NJB, Cox MAJ, Bouten CVC, Baaijens FPT (2008) Remodelling of the angular collagen fiber distribution in cardiovascular tissues. Biomech Model Mechanobiol 7:93–103. doi: 10.1007/s10237-007-0078-x

Driessen NJB, Wilson W, Bouten CVC, Baaijens FPT (2004) A computational model for collagen fibre remodelling in the arterial wall. J Theor Biol 226:53–64. doi: 10.1016/j.jtbi.2003.08.004

Ferizi U, Rossi I, Lee Y, et al (2016) Diffusion tensor imaging of articular cartilage at 3T correlates with histology and biomechanics in a mechanical injury model. Magn Reson Med. doi: 10.1002/mrm.26336

Gilbert S, Chen T, Hutchinson ID, et al (2014) Dynamic contact mechanics on the tibial plateau of the human knee during activities of daily living. J Biomech 47:2006–2012. doi: 10.1016/j.jbiomech.2013.11.003

Hariton I, de Botton G, Gasser TC, Holzapfel G a (2007) Stress-driven collagen fiber remodeling in arterial walls. Biomech Model Mechanobiol 6:163–75. doi: 10.1007/s10237-006-0049-7

Hart DJ, Spector TD, Law M, Doyle D V. (1991) The relationship between osteoarthritis (Oa) and osteoporosis in the general population: The chingford study. Rheumatol (United Kingdom) 30:55. doi: 10.1093/rheumatology/XXX.suppl_2.52

Heinemeier KM, Schjerling P, Heinemeier J, et al (2016) Radiocarbon dating reveals minimal collagen turnover in both healthy and osteoarthritic human cartilage. Sci Transl Med 8:346ra90. doi: 10.1126/scitranslmed.aad8335

Hosseini SM, Wilson W, Ito K, van Donkelaar CC (2014) A numerical model to study mechanically induced initiation and progression of damage in articular cartilage. Osteoarthritis Cartilage 22:95–103. doi: 10.1016/j.joca.2013.10.010

Julkunen P, Kiviranta P, Wilson W, et al (2007) Characterization of articular cartilage by combining microscopic analysis with a fibril-reinforced finite-element model. J Biomech 40:1862–70. doi: 10.1016/j.jbiomech.2006.07.026

Karsdal MA, Madsen SH, Christiansen C, et al (2008) Cartilage degradation is fully reversible in the presence of aggrecanase but not matrix metalloproteinase activity. Arthritis Res Ther 10:R63. doi: 10.1186/ar2434

Kłodowski A, Mononen ME, Kulmala JP, et al (2016) Merge of motion analysis, multibody dynamics and finite element method for the subject-specific analysis of cartilage loading patterns during gait: differences between rotation and moment-driven models of human knee joint. Multibody Syst Dyn 37:271–290. doi: 10.1007/s11044-015-9470-y

Korhonen RK, Tanska P, Kaartinen SM, et al (2015) New Concept to Restore Normal Cell Responses in Osteoarthritic Knee Joint Cartilage. Exerc Sport Sci Rev 43:143–52. doi: 10.1249/JES.0000000000000051

Kääb MJ, Ito K, Clark JM, Nötzli HP (1998) Deformation of articular cartilage collagen structure under static and cyclic loading. J Orthop Res 16:743–51. doi: 10.1002/jor.1100160617

Lanir Y (2015) Mechanistic micro-structural theory of soft tissues growth and remodeling: tissues with unidirectional fibers. Biomech Model Mechanobiol 14:245–266. doi: 10.1007/s10237-014-0600-x

Li J, Hua X, Jin Z, et al (2014) Biphasic investigation of contact mechanics in natural human hips during activities. Proc Inst Mech Eng Part H J Eng Med 228:556–563. doi: 10.1177/0954411914537617

Li Y, Frank EH, Wang Y, et al (2013) Moderate dynamic compression inhibits pro-catabolic response of cartilage to mechanical injury, tumor necrosis factor-α and interleukin-6, but accentuates degradation above a strain threshold. Osteoarthritis Cartilage 21:1933–41. doi: 10.1016/j.joca.2013.08.021

Lohmander S (1988) Proteoglycans of joint cartilage. Structure, function, turnover and role as markers of joint disease. Baillieres Clin Rheumatol 2:37–62. doi: S0950-3579(88)80004-9 [pii]

Lyman JR, Chappell JD, Morales TI, et al (2012) Response of Chondrocytes to Local Mechanical Injury in an *Ex Vivo* Model. Cartilage 3:58–69. doi: 10.1177/1947603511421155

Maroudas A, Bayliss MT, Uchitel-Kaushansky N, et al (1998) Aggrecan turnover in human articular cartilage: use of aspartic acid racemization as a marker of molecular age. Arch Biochem Biophys 350:61–71. doi: 10.1006/abbi.1997.0492

Menzel A (2007) A fibre reorientation model for orthotropic multiplicative growth. Configurational driving stresses, kinematics-based reorientation, and algorithmic aspects. Biomech Model Mechanobiol 6:303–20. doi: 10.1007/s10237-006-0061-y

Miramini S, Smith DW, Zhang L, Gardiner BS (2017) The spatio-temporal mechanical environment of healthy and injured human cartilage during sustained activity and its role in cartilage damage. J Mech Behav Biomed Mater 74:1–10. doi: 10.1016/j.jmbbm.2017.05.018

Mononen ME, Tanska P, Isaksson H, Korhonen RK (2016) A Novel Method to Simulate the Progression of Collagen Degeneration of Cartilage in the Knee: Data from the Osteoarthritis Initiative. Sci Rep 6:21415. doi: 10.1038/srep21415

Mow VC, Guo XE (2002) Mechano-electrochemical properties of articular cartilage: their inhomogeneities and anisotropies. Annu Rev Biomed Eng 4:175–209. doi: 10.1146/annurev.bioeng.4.110701.120309

Myller KAH, Turunen MJ, Honkanen JTJ, et al (2016) In Vivo Contrast-Enhanced Cone Beam CT Provides Quantitative Information on Articular Cartilage and Subchondral Bone. Ann Biomed Eng. doi: 10.1007/s10439-016-1730-3

Nagel T, Ph D, Kelly DJ, et al (2013) The composition of engineered cartilage at the time of implantation determines the likelihood of regenerating tissue with a normal collagen architecture. Tissue Eng Part A 0:824–33. doi:

10.1089/ten.TEA.2012.0363

Neuman P, Dahlberg LE, Englund M, Struglics A (2017) Concentrations of synovial fluid biomarkers and the prediction of knee osteoarthritis 16 years after anterior cruciate ligament injury. Osteoarthr Cartil 25:492–498. doi: 10.1016/j.joca.2016.09.008

Oomen PJA, Loerakker S, Van Geemen D, et al (2016) Age-dependent changes of stress and strain in the human heart valve and their relation with collagen remodeling. Acta Biomater 29:161–169. doi: 10.1016/j.actbio.2015.10.044

Quiroga JMP, Wilson W, Ito K, van Donkelaar CC (2017) Relative contribution of articular cartilage's constitutive components to load support depending on strain rate. Biomech Model Mechanobiol 16:151–158. doi: 10.1007/s10237-016-0807-0

Rachev A, Manoach E, Berry J, Moore JE (2000) A Model of Stress-induced Geometrical Remodeling of Vessel Segments Adjacent to Stents and Artery/Graft Anastomoses. J Theor Biol 206:429–443. doi: 10.1006/jtbi.2000.2143

Raub CB, Hsu SC, Chan EF, et al (2013) Microstructural remodeling of articular cartilage following defect repair by osteochondral autograft transfer. Osteoarthr Cartil 21:860–868. doi: 10.1016/j.joca.2013.03.014

Rolauffs B, Muehleman C, Li J, et al (2010) Vulnerability of the superficial zone of immature articular cartilage to compressive injury. Arthritis Rheum 62:3016–27. doi: 10.1002/art.27610

Saarakkala S, Julkunen P, Kiviranta P, et al (2010) Depth-wise progression of osteoarthritis in human articular cartilage: investigation of composition, structure and biomechanics. Osteoarthritis Cartilage 18:73–81. doi: 10.1016/j.joca.2009.08.003

Sasazaki Y, Shore R, Seedhom BB (2006) Deformation and failure of cartilage in the tensile mode. J Anat 208:681–694. doi: 10.1111/j.1469-7580.2006.00569.x

Soltz MA, Ateshian GA (2000) A Conewise Linear Elasticity mixture model for the analysis of tension-compression nonlinearity in articular cartilage. J Biomech Eng 122:576–86.

Stoop R, van der Kraan PM, Buma P, et al (1999) Denaturation of type II collagen in articular cartilage in experimental murine arthritis. Evidence for collagen degradation in both reversible and irreversible cartilage damage. J Pathol 188:329–37. doi: 10.1002/(SICI)1096-9896(199907)188:3<329::AID-PATH371>3.0.CO;2-B

Taber LA, Humphrey JD (2001) Stress-Modulated Growth, Residual Stress, and Vascular Heterogeneity. J Biomech Eng 123:528. doi: 10.1115/1.1412451

Tanska P, Mononen ME, Korhonen RK (2015) A multi-scale finite element model for investigation of chondrocyte mechanics in normal and medial meniscectomy human knee joint during walking. J Biomech 48:1397–406. doi: 10.1016/j.jbiomech.2015.02.043

Tanska P, Turunen SM, Han S-K, et al (2013) Superficial collagen fibril modulus and pericellular fixed charge density modulate chondrocyte volumetric behaviour in early osteoarthritis. Comput Math Methods Med 2013:164146. doi: 10.1155/2013/164146

Teeple E, Elsaid KA, Fleming BC, et al (2008) Coefficients of friction, lubricin, and cartilage damage in the anterior cruciate ligament-deficient guinea pig knee. J Orthop Res 26:231–7. doi: 10.1002/jor.20492

van der Voet A (1997) A comparison of finite element codes for the solution of biphasic poroelastic problems. Proc Inst Mech Eng H 211:209–11.

Venäläinen MS, Mononen ME, Jurvelin JS, et al (2014) Importance of Material Properties and Porosity of Bone on Mechanical Response of Articular Cartilage in Human Knee Joint - A Two-Dimensional Finite Element Study. J Biomech Eng 136 (12):1–8.

Venäläinen MS, Mononen ME, Salo J, et al (2016) Quantitative Evaluation of the Mechanical Risks Caused by Focal Cartilage Defects in the Knee. Sci Rep 6:37538. doi: 10.1038/srep37538

Virén T, Timonen M, Tyrväinen H, et al (2012) Ultrasonic evaluation of acute impact injury of articular cartilage in vitro. Osteoarthritis Cartilage 20:719–26. doi: 10.1016/j.joca.2012.03.018

Wilson W, Driessen NJB, van Donkelaar CC, Ito K (2006) Prediction of collagen orientation in articular cartilage by a collagen remodeling algorithm. Osteoarthritis Cartilage 14:1196–202. doi: 10.1016/j.joca.2006.05.006

Wilson W, van Donkelaar CC, van Rietbergen B, et al (2004) Stresses in the local collagen network of articular cartilage: a poroviscoelastic fibril-reinforced finite element study. J Biomech 37:357–366. doi: 10.1016/S0021-9290(03)00267-7

Wilson W, van Donkelaar CC, van Rietbergen B, et al (2005a) Erratum to “Stresses in the local collagen network of articular cartilage: a poroviscoelastic fibril-reinforced finite element study” [Journal of Biomechanics 37 (2004) 357–366] and “A fibril-reinforced poroviscoelastic swelling model for articular cartil. J Biomech 38:2138–2140. doi: 10.1016/j.jbiomech.2005.04.024

Wilson W, van Donkelaar CC, van Rietbergen B, Huiskes R (2005b) A fibril-reinforced poroviscoelastic swelling model for articular cartilage. J Biomech 38:1195–204. doi: 10.1016/j.jbiomech.2004.07.003

Yang NH, Nayeb-Hashemi H, Canavan PK, Vaziri A (2010) Effect of frontal plane tibiofemoral angle on the stress and strain at the knee cartilage during the stance phase of gait. J Orthop Res 28:1539–1547. doi: 10.1002/jor.21174

Zhang L, Miramini S, Smith DW, et al (2015) Time evolution of deformation in a human cartilage under cyclic loading. Ann Biomed Eng 43:1166–77. doi: 10.1007/s10439-014-1164-8

APPENDIX A: SUPPLEMENTARY MATERIAL

2. Materials and methods

2.1 Material model

2.1.1 Implementation of the collagen fibril network architechture

As stated in the paper, the collagen fibril network incorporated 4 primary and 13 secondary fibrils. Primary fibrils define Benninghoff-type collagen fibril architecture (Benninghoff 1925) while the secondary fibrils describe randomly organized fibrils and collagen cross-links. The fibril orientation angle (θ) is now a function of the normalized distance from the cartilage surface (z; z = 0 at cartilage surface and z = 1 at bone-cartilage interface) and can be presented as follows:

$$\theta = \begin{cases} 0, & z \leq d_{\mathrm{sup}}, \\ \dfrac{\arctan(z)}{d_{\mathrm{mid}} - \sqrt{\left(d_{\mathrm{mid}}^2 - (z - d_{\mathrm{mid}})^2\right)}}, & d_{\mathrm{sup}} < z < d_{\mathrm{sup}} + d_{\mathrm{mid}}, \\ \dfrac{\pi}{2}, & z \geq d_{\mathrm{sup}} + d_{\mathrm{mid}}, \end{cases} \tag{A.1}$$

where d_{sup} and d_{mid} are relative thicknesses of the superficial and middle zones of cartilage, respectively (Supplementary figure 1). In the 3D case, the fibril is then rotated 90° three additional times to ensure symmetry of the fibril architecture. A value for z can be formed from a normalized resultant of a direction vector from an arbitrary nodal point to the closest point in the cartilage surface. The calculated orientation values are then interpolated to the integration points of the

elements.

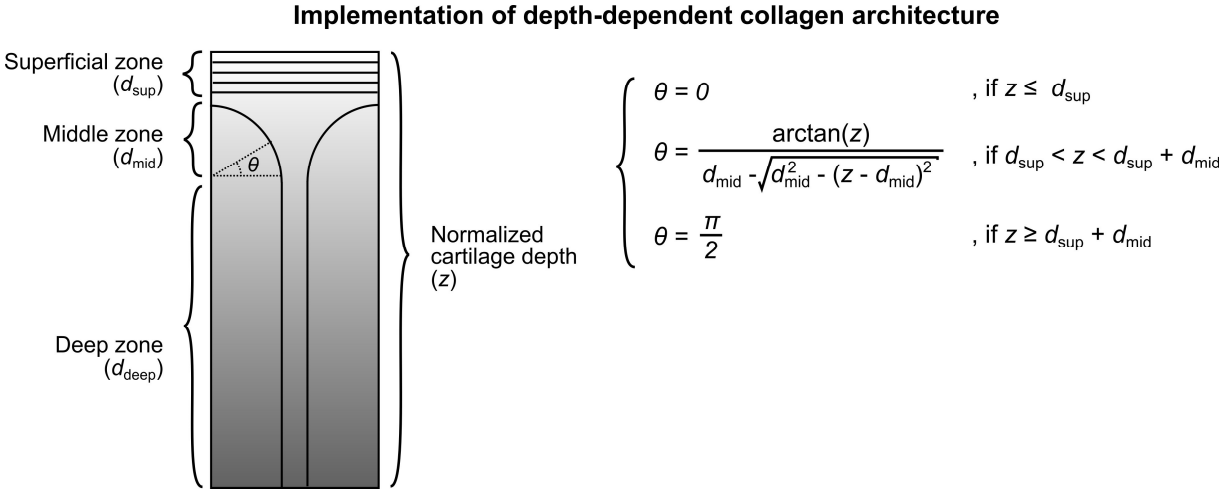

Supplementary figure 1: Representation of the "Benninghoff type" arcade fibril architecture (Benninghoff 1925) implemented into the model. θ is the orientation angle of the fibril, z is the normalized cartilage depth (normalized distance from the cartilage surface; 0 = cartilage surface; 1 = bone cartilage interface), d_{sup} and d_{mid} are the (normalized) thicknesses of the superficial and middle (translational) zone, respectively. In the 3D case, the fibril is then rotated $\pi/2$ (*i.e.* 90°) three additional times to ensure symmetry of the fibril architecture.

References

Benninghoff A (1925) Form und Bau der Gelenkknorpel in ihren Beziehungen zur Funktion. Z Anat Entwicklungsgesch 76:43–63. doi: 10.1007/BF02134417